Island size distribution with hindered aggregation

Diego Luis González,[1,*] Manuel Camargo,[2,†] and Julián A. Sánchez[1,‡]

[1]*Departamento de Física, Universidad del Valle, A.A. 25360, Cali, Colombia*
[2]*CICBA, Universidad Antonio Nariño–Campus Farallones, Km 18 vía Cali-Jamundí, Cali, Colombia*

We study the effect of hindered aggregation on the island formation processes for a one-dimensional model of epitaxial growth with arbitrary nucleus size i. In the proposed model, the attachment of monomers to islands is hindered by an aggregation barrier, ϵ_a, which decreases the hopping rate of monomers to the islands. As ϵ_a increases, the system exhibits a crossover between two different regimes; namely, from diffusion-limited aggregation to attachment-limited aggregation. The island size distribution, $P(s)$, is calculated for different values of ϵ_a by a self-consistent approach involving the nucleation and aggregation capture kernels. The results given by the analytical model are compared with those from kinetic Monte Carlo simulations, finding a close agreement between both sets of data for all considered values of i and ϵ_a. As the aggregation barrier increases, the spatial effect of fluctuations on the density of monomers can be neglected and $P(s)$ smoothly approximates to the limit distribution $P(s) = \delta_{s,i+1}$. In the crossover regime the system features a complex and rich behavior, which can be explained in terms of the characteristic timescales of different microscopic processes.

I. INTRODUCTION

Epitaxial growth (EG) has long been a subject of study due to both its academic and industrial importance. From an academic point of view, this out-of-equilibrium process is interesting as it displays a rich and complex behavior arising from the several timescales involved [1–14]. On the other hand, an understanding of the microscopic mechanisms affecting the growth process is a requirement to achieve an accurate description of material properties in industrial applications. A typical example of the latter is the use of atomic chains in nanoscale devices, life sciences, and fuel cells [15–17] which can be formed, for example, by using stepped surfaces [18,19] or by anisotropic diffusion on two-dimensional substrates [20–23].

In general terms, the microscopic mechanisms of EG involve three basic processes: nucleation, aggregation, and transport of basic growth units, usually referred to as monomers, which may be atoms, molecules, or colloidal particles. During EG, monomers are deposited onto a flat substrate or a stepped surface at a constant deposition rate, F. The latter is well controlled in experimental setups and therefore can be considered as a known parameter in theoretical models. The time evolution of the deposition process is normally described in terms of the coverage θ, which is defined as the number of monomers per lattice site on the substrate at time t. If evaporation of monomers from substrate is negligible, then $\theta \approx Ft$. After its deposition, a monomer diffuses on the substrate with (lateral) diffusion constant D until they nucleate or aggregate. Nucleation occurs when a number of monomers

form an island, i.e., a stable cluster, and the aggregation process takes place when a monomer attaches to a previously nucleated island.

A paramount concept in standard models of epitaxial growth is that of the critical nucleus size i, which is defined as the size of the largest unstable cluster, i.e., clusters with size larger than i are static and stable. Consequently clusters with size smaller than $i + 1$ are considered unstable and the monomers belonging to such clusters can diffuse away with diffusion constant D. Therefore, each monomer forming an unstable cluster behaves as a free monomer. In most EG models, nucleation and aggregation are instantaneous processes, i.e., monomers are incorporated to the clusters once they reach the interaction range; in such a case, the aggregation belongs to the diffusion-limited-aggregation (DLA) regime. Nevertheless, in more realistic situations nucleation and/or aggregation could be hindered by additional energy barriers which would increase the time required for each reaction.

For instance, experiments on nucleation and growth of Ge islands on a Pb overlayer covering a Si(111) surface suggest that such a barrier could appear due to strain [24–27]. Also, nucleation hindered by attachment barriers has been observed in Fe deposition on graphene [28] and in metal (111) homoepitaxial systems [29,30]. Similarly, attachment barriers must be considered to properly explain the formation of graphene sheets on metal [31–34] and oxide [35] substrates. In the former case, individual graphene islands spread at a constant rate, suggesting that their growth is controlled by the attachment rate of carbon adatoms to the island edges.

Motivated by previous theoretical [2,3,12,14,36–46] and experimental [21,22,47–51] studies, in this work we propose a one-dimensional model in which the aggregation of monomers is hindered by an additional attachment barrier ϵ_a. As explained in the next sections, this barrier decreases the hopping rate of monomers to islands. Thus, for large barriers the monomers

*diego.luis.gonzalez@correounivalle.edu.co

†manuel.camargo@uan.edu.co

‡julian.a.sanchez@correounivalle.edu.co
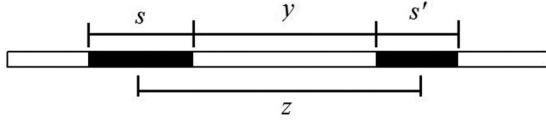
FIG. 1. Two adjacent islands (black segments) with lengths s and s'. The length of the gap between island edges is y, while the distance between their centers is z.

need many attempts to be incorporated into the islands. In this case, the aggregation is attachment limited and the system is in the attachment-limited-aggregation (ALA) regime. Naturally, for zero and weak barriers, our model recovers the widely studied DLA regime. Although an attachment barrier could also be considered for unstable clusters (see Ref. [52]), we neglect it to keep our approach as one of the simplest models from which we can learn some general properties of systems exhibiting a crossover between DLA and ALA.

One-dimensional models have distinctive features which make them amenable to theoretical treatment. For example, islands in a one-dimensional (1D) defect-free flat substrate unambiguously split it into independent segments called gaps, as schematically shown in Fig. 1. A monomer deposited inside of a particular gap must eventually either aggregate to one of the islands delimiting the gap, or coalesce with an unstable cluster to nucleate a new island and therefore form two new gaps. Furthermore, the 1D model allows the explicit calculation of several quantities of interest (e.g., capture kernels as a function of the capture zone length, gap length distribution in terms of the nucleation rate, etc.). There are several ways to represent islands in EG models. In the so-called "point-island model," all monomers belonging to an island are on top of each other on the same lattice site and the island size is given just by the number of monomers, s, attached to it. On the other hand, in the "extended-island model," the islands growth laterally and the size of an island are given by the length between its edges as shown in Fig. 1.

As previously mentioned, several timescales are involved in epitaxial growth. In order to simplify the discussion, let us consider a single gap of length y (see Fig. 1). The average time between consecutive depositions inside the gap is τ_{dep} and the typical time of the first encounter between a monomer and the edge of an island is τ_{tr}. The aggregation barrier ϵ_a defines the aggregation time, τ_a, i.e., the typical time that a single monomer spends inside the gap. If $\tau_a \approx \tau_{\text{tr}}$ the system is in the realm of the DLA regime; in the opposite case, when large barriers are considered, $\tau_a \gg \tau_{\text{tr}}$ and consequently the system is set in the ALA regime. It is also possible to define the typical time of nucleation τ_n. Naturally, the ratio between these timescales depends directly on the size of the gap y and determines the physical properties of the system [36–41,52–57].

A further important quantity for modeling EG is the island size distribution, $P(s)$. In the case of two-dimensional (2D) systems, $P(s)$ can be measured experimentally and used to extract information regarding the underlying microscopic processes [58,59]. Up to now, most theoretical investigations have been mainly focused on the DLA regime. Among the few studies considering the ALA regime, one of the most

prominent for 2D islands is Ref. [60], where a novel behavior for the density of islands was found as a function of the flux F and temperature T, explaining experimental results which were inconsistent with the standard DLA theory. Recent works have presented significant results in the ALA regime for some quantities such as the densities of monomers and islands, the capture zone, and gap size distributions [36–38,52]. However, almost nothing has been said about the behavior of $P(s)$. In the present paper, we report a detailed analysis of the island size distribution for a 1D model, which exhibits a crossover between DLA and ALA regimes.

This paper is organized as follows: Sec. II summarizes the general framework used to calculate the quantities of interest, i.e., the density of free monomers, the average density of islands, and the island size distribution. Section III presents a model where the attachment of monomers to islands is hindered by an additional barrier. Finally, the analytical results are compared with those from numerical simulations in Sec. IV, where we also draw our conclusions.

II. ANALYTICAL MODEL

A. Rate equations

As mentioned above, this work is focused on the island size distribution, which is defined as $P(s) = N_s/N$, where N_s represents the average density of islands with size $s > i$ and $N = \sum_{s \geqslant i+1} N_s$ is the total island density. On the other hand, the density of free monomers N_1 is expressed in terms of the density η_s of unstable clusters with size $1 \leqslant s \leqslant i$, according to $N_1 = \sum_{s=1}^{i} \eta_s$. The time evolution of N_1 and N_s can be described by standard rate equations (REs) [12–14,46,61].

In terms of the coverage, the RE for N_1 can be written as

$$\frac{dN_1}{d\theta} = \gamma - (i+1)\sigma_u \Re N_1 \eta_i - \Re N_1 \sum_{s \geqslant i+1} \sigma_s N_s, \quad (1)$$

where γ is the fraction of the substrate which is not covered by islands. Thus, $\gamma = 1 - \theta + N_1$ for the extended-island model and $\gamma = 1 - N$ for the point-island model. The second term of Eq. (1) represents nucleation while the third one takes into account the aggregation. Note that we have neglected the direct deposition onto occupied lattice sites and consequently, in our simulations only depositions on empty sites are allowed. The constant $\Re = D/F$ is the ratio between the diffusion constant and the deposition rate. In the experimental setup, the diffusion constant D is usually much larger than F; then, from now on, we set $\Re = 5 \times 10^6$ for numerical calculations. The coverage-dependent factors σ_u and σ_s are the capture kernels for unstable clusters of size i and islands, respectively. From now on, the subscript u stands for unstable.

Similarly, the evolution of N_s is given by

$$\frac{dN_s}{d\theta} = \Re N_1(\sigma_{s-1}N_{s-1} - \sigma_s N_s), \quad (2)$$

where $\sigma_{s=i} = \sigma_u$ and $N_i = \eta_i$. The terms on the right side of Eq. (2) represent the aggregation of monomers to islands with size $s-1$ and s, respectively. The evolution of the total density of islands is obtained by summing Eq. (2) over $s > i$, resulting

in

$$\frac{dN}{d\theta} = \sigma_u \Re N_1 \eta_i. \tag{3}$$

In order to make analytical progress, the Walton's relation is used to write $\eta_i \approx N_1^i$ [62,63]. Defining the average capture kernel as

$$\bar{\sigma} = \frac{1}{N} \sum_{s \geqslant i+1} \sigma_s N_s, \tag{4}$$

we obtain

$$\frac{dN_1}{d\theta} = \gamma - (i+1)\Re \sigma_u N_1^{i+1} - \bar{\sigma}\Re N_1 N \tag{5}$$

and

$$\frac{dN}{d\theta} = \Re \sigma_u N_1^{i+1}. \tag{6}$$

An equivalent way to write Eqs. (5) and (6) is introducing the nucleation and monomer capture lengths, which are denoted as ξ_u and ξ, respectively. By using the capture lengths, Eqs. (5) and (6) take the form

$$\frac{dN_1}{d\theta} = \gamma - \Re \frac{N_1}{\xi^2} \tag{7}$$

and

$$\frac{dN}{d\theta} = \Re \frac{N_1}{(i+1)\xi_u^2}. \tag{8}$$

This set of differential equations is usually called "contracted" RE [14]. The relation between capture kernels and lengths can be easily obtained comparing Eqs. (5) and (6) with their contracted counterparts. Therefore

$$\frac{1}{\xi^2} = \frac{1}{\xi_u^2} + \sum_{s \geqslant i+1} \sigma_s N_s \tag{9}$$

and

$$\frac{1}{\xi_u^2} = (i+1)\sigma_u N_1^i. \tag{10}$$

The monomer capture length and the timescales τ_a and τ_n are related according to

$$\frac{1}{\xi^2} = \frac{N}{D N_1} \left((i+1) \left\langle \frac{\bar{n}_1 y}{\tau_n} \right\rangle + \left\langle \frac{\bar{n}_1 y}{\tau_a} \right\rangle \right), \tag{11}$$

where $\langle \cdot \rangle$ represents the average over the gaps ensemble and $\bar{n}_1$ is the average density of (free) monomers inside the gap of length y.

The RE are equivalently defined by the capture kernels, the capture lengths, or the timescales τ_n and τ_a. If one of these sets of parameters is known, then the densities N and N_1 can be obtained from the numerical solution of the corresponding RE. However, the calculation of the island size distribution $P(s)$ is more involved because the dependence of the capture kernels on the size of the islands has to be taken into account. In other words, the size-dependent kernels σ_s must be explicitly calculated rather than simply the average kernel $\bar{\sigma}$.

Perhaps, the simplest nontrivial case corresponds to constant kernels, i.e., size- and coverage-independent kernels.

Taking $\sigma_u(\theta) = \sigma_u, \sigma_s(\theta) = \sigma$ and defining $\tau = \sigma \Re \int_0^\theta N_1 d\theta'$, Eq. (2) can be rewritten as

$$\frac{dN_{i+1}}{d\tau} = \frac{\sigma_u}{\sigma} N_1^i - N_{i+1}, \tag{12}$$

$$\frac{dN_s}{d\tau} = N_{s-1} - N_s \qquad \text{for } s > i+1. \tag{13}$$

For large coverages the solution of Eq. (13) can be approximated by (see Appendix)

$$N_{s+i+1} \approx \frac{\sigma_u}{\sqrt{\pi}\sigma} \int_z^\infty dv \, \exp(-v^2)[\sqrt{2\tau}(v-z)]^{-[i\chi(1+\chi)]}, \tag{14}$$

where χ is a growth exponent defined by $N_1 \propto \theta^\chi$ and $z = (s - \tau)/\sqrt{2\tau}$. The realm of validity of Eq. (14) is discussed in Sec. IV.

In general, the capture kernel of an island depends on both the coverage and the island size. For those cases Eq. (14) does not apply. As described below, the standard procedure used to calculate σ_s is based on the solution of a self-consistent set of equations, which in turn are rooted in an approximate description of the nucleation process.

B. Self-consistent approach for capture kernels

Given its importance, the functional form of $P(s)$ in the DLA regime has been discussed in many previous works. Based on scaling arguments and numerical evidence, semiempirical distributions have been employed to describe the distribution of cluster sizes [64–66]. For instance, Amar and Family suggested a coverage-independent distribution given by

$$P(s) = A_i s^i \exp(-i B_i x^{1/B_i}), \tag{15}$$

where C_i and a_i are fitting parameters depending on the critical nucleus size i. Also, some analytical expressions relating $P(s)$ to the capture kernels have been proposed [8,10,46,67]. Based on a continuum limit of the RE, Bartelt and Evans obtained the expression

$$P(s) = P(0) \exp \left(\int_0^s dx \frac{(2C_1 - 1) - \frac{dC}{dx}}{C(x) - C_2 x} \right), \tag{16}$$

where C_1 and C_2 are fit parameters close to $\partial(\ln \bar{s})/\partial(\ln \theta)$, and $C(s) \approx \sigma_s/\bar{\sigma}$ [67]. This expression is not hard to evaluate but requires the capture kernels σ_s as input. More general— although not explicit—expressions to calculate $P(s)$ can also be found by means of a self-consistent (SC) method which involves the kernels σ_s and σ_u as inputs. This approach has been successfully used for the case $i = 1$ in the DLA regime [13,14]; nevertheless, the SC method is quite general and can be applied to more general models of epitaxial growth, as summarized in the following.

Let z be the distance between the center of an island with length s and the center of the adjacent island at the right. The associated gap length between these adjacent islands is y as shown in Fig. 1. For point islands we consider $y \approx z$, while for extended islands we assume that there exists no correlation between the size of adjacent islands. Under this assumption, the relation between y and z can be approximated by $y \approx z - (s + \bar{s})/2$ with $\bar{s} = (\theta - N_1)/N$ the average island size.

The distribution $p_s(z; \theta)$ is defined as the probability density to find an island with size s and distance between adjacent centers z. Neglecting the effect of the deposition of monomers on top of the islands and the breakup of gaps due to nucleation, the set of equations for the time evolution of $p_s(z, \theta)$ is given by

$$\frac{dp_{i+1}(z; \theta)}{d\theta} = \frac{dN}{d\theta} \delta(z - \bar{z}) - \Re N_1 \tilde{\sigma}_{i+1}(y) p_{i+1}(z; \theta) \quad (17)$$

and

$$\frac{dp_s(z; \theta)}{d\theta} = \Re N_1 [\tilde{\sigma}_{s-1}(y) p_{s-1}(z; \theta) - \tilde{\sigma}_s(y) p_s(z; \theta)], \quad (18)$$

with $s > i + 1$ [14]. The first term of Eq. (17) represents nucleation. Note that the Dirac delta function $\delta(z - \bar{z})$ implies that the length of the new gaps generated by nucleation is always equal to the average gap size $\bar{y} = \gamma/N$. The additional terms in Eqs. (17) and (18) represent the aggregation of monomers to islands. Defining θ_z according to $z = 1/N(\theta_z)$, it is possible to write Eq. (17) as

$$\frac{dp_{i+1}(z; \theta)}{d\theta} = \frac{1}{z^2} \delta(\theta - \theta_z) - \Re N_1 \tilde{\sigma}_{i+1}(y) p_{i+1}(z; \theta). \quad (19)$$

By definition, $\tilde{\sigma}_s(y_s)$ is the local capture kernel of an island of size s with an associated gap of length y_s. Thus, the kernels σ_s which appear in the RE are the average over the gap lengths of $\tilde{\sigma}_s(y_s)$. For point islands, the capture kernels have no explicit dependence on the island size. However, for extended islands the explicit dependence on the island size s in the capture kernels does not allow one to analytically solve Eqs. (18) and (19). Nevertheless, the capture kernels for extended islands can be approximated by $\tilde{\sigma}_s(y) \approx \tilde{\sigma}_{\bar{s}}(y) = \tilde{\sigma}_{\bar{s}}(z - \bar{s})$. Consequently, for both point and extended islands it becomes possible to use the transformation,

$$X_z = \Re \int_{\theta_z}^{\theta} N_1(\theta') \tilde{\sigma}_s(z) d\theta', \quad (20)$$

to find the solution of Eqs. (18) and (19). In terms of the new variable X_z, the explicit solution is given by [14]

$$p_s(z; X_z) = \frac{X_z^{s-(i+1)} \exp(-X_z)}{z^2 [s - (i+1)]!}. \quad (21)$$

The average value of z for a given s, $\bar{z}_s$, can be calculated from

$$\bar{z}_s = \frac{\sum_z z p_s(z; X_z)}{\sum_z p_s(z; X_z)}. \quad (22)$$

For large coverages, i.e., beyond the nucleation regime, $p_s(z; X_z)$ is a sharply peaked distribution of z and therefore the capture kernels can be approximated by

$$\sigma_s = \frac{\sum_z \tilde{\sigma}_s(z) p_s(z; X_z)}{\sum_z p_s(z; X_z)} \approx \tilde{\sigma}_s(\bar{z}_s). \quad (23)$$

Note that it is also possible to use the peak position z^* in Eq. (23) instead of $\bar{z}_s$ to approximate the capture kernels [13,14]. We found similar results by using both procedures; nevertheless, from the computational point of view, it is more convenient to find $\bar{z}_s$ than z_s^*. The average value of z_s calculated from Eq. (22) is larger than the correct value since the effect of the breakup due to nucleation has been neglected in Eqs. (17)–(19). To include the nucleation effect, it

is necessary to rescale the length to ensure the correct average value $\bar{z} = \gamma/N = \sum_s z_s N_s/N$. Using

$$\tilde{z}_s = \frac{\gamma \bar{z}_s}{\sum_s \bar{z}_s N_s}, \quad (24)$$

the capture kernels σ_s appearing in the RE are finally given by

$$\sigma_s = \tilde{\sigma}_s \left(\tilde{z}_s - \frac{s + \bar{s}}{2} \right), \quad (25)$$

for extended islands, while $\sigma_s = \tilde{\sigma}(\tilde{z}_s)$ for point islands.

In summary, the procedure to determine N_1 and N_s is the following: if the local capture kernel $\tilde{\sigma}_s(y)$ is known, at each discrete time step the integral given by Eq. (20) can be calculated. Then the values of $\bar{z}_s$ are found from Eqs. (21) and (22) for all relevant values of s. Afterward, the size-dependent capture kernels, σ_s, can be calculated using Eqs. (24) and (25). Finally, Eqs. (2) and (5) are integrated to find the densities of monomers and islands at the next time step. This self-consistent procedure is schematically represented in Fig. 2. For small coverages, where the distribution $p_s(z; X_z)$ does not feature a well-defined peak, the RE can be solved by means of the mean-field (MF) approximation $\sigma_s \approx \bar{\sigma}$ for all s. In this approximation, the dependence on the island size of σ_s is neglected and the capture kernels just depend on the coverage.

In the next section the local capture kernel $\tilde{\sigma}_s(y)$ as well as the nucleation kernel σ_u are calculated for a model of EG where the aggregation of monomers to islands is hindered by an additional barrier.

III. ISLAND FORMATION WITH HINDERED AGGREGATION

In standard EG models free monomers diffuse on the substrate with a hopping rate $r = 2D$ until they are captured by an island (aggregation) or by an unstable cluster of size i (nucleation). Similarly, monomers belonging to unstable clusters can diffuse away with a hopping rate r. However, the hopping rate to stable islands is hindered by an additional attachment barrier ϵ_a which reduces the hopping rate to those islands to $r' = 2D'$. As usual, ϵ_a has an associated characteristic length $l_a = \exp(\epsilon_a/k_B T) - 1$ which determines the asymmetry between D and D' as $D/D' = l_a + 1$ [36–38,52,55]. As previously mentioned, for the sake of simplicity we neglect the deposition on occupied sites, which constrains the applicability of our model to the low coverage regime. The island size distributions reported here were evaluated at coverages up to $\theta_{\max} = 0.25$. For this value of coverage, the fraction of empty sites on the substrate is about 95% for point islands and 80% for extended islands. Thus, the deposition on top of stable islands is negligible especially for point islands, where it is below 5%.

The behavior of the system depends on the relevant timescales. For a single gap of length y, the average time between consecutive depositions is given by $\tau_{\mathrm{dep}} = (Fy)^{-1}$, while the average aggregation time can be expressed as [39–41,55]

$$\tau_a = \frac{y}{12D}(y + 6l_a). \quad (26)$$
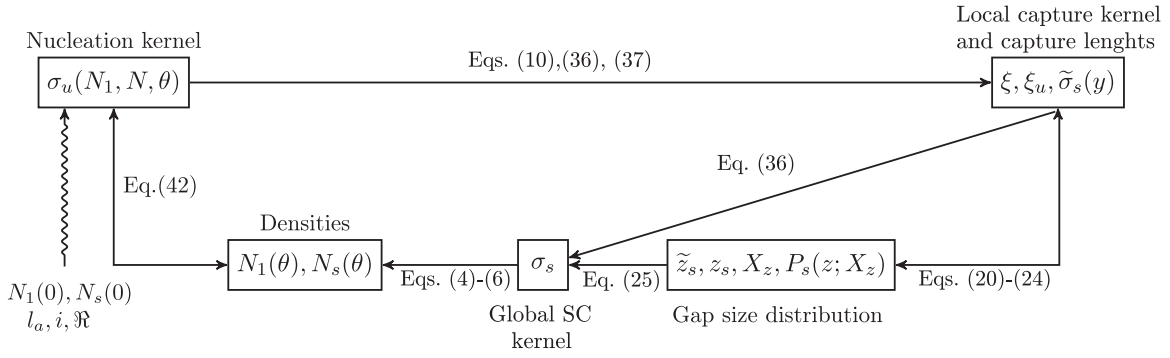
FIG. 2. Schematic representation of the SC procedure to determine N_1 and N_s.

The transversal time can be calculated taking $l_a = 0$ in last equation, i.e., $\tau_{\mathrm{tr}} = y^2/(12D)$. In the DLA regime $\tau_{\mathrm{dep}} \gg \tau_a \approx \tau_{\mathrm{tr}}$, while in the ALA regime $\tau_{\mathrm{dep}} \gg \tau_a \gg \tau_{\mathrm{tr}}$.

During the low coverage regime (L), monomers diffuse in such a way that nucleation and aggregation are rare events and $N_1 \approx \theta$. The attachment barrier has no effect because ϵ_a only affects aggregation of monomers to islands. On the other hand, for large times most of the monomers aggregate to islands and nucleation is negligible, defining the aggregation regime (A). The time evolution of the system on the A regime strongly depends on ϵ_a. In both L and A regimes, scaling forms $N_1 \propto \theta^\chi$ and $N \propto \theta^\beta$ are expected with χ and β noninteger exponents. The crossover between L and A occurs at coverage θ_c which depends on $\Re$, i, and l_a. For large barriers, between L and A regimes an intermediate regime is found where $N \approx \theta/(i+1)$ and N_1 is almost constant, as explained in detail in Ref. [38].

The kernel $\bar{\sigma}$ can be calculated considering the evolution of the spatial average of the local density of monomers $\bar{n}_1$ inside a single gap with size y in the aggregation regime where nucleation is negligible. In this regime,

$$\frac{d\bar{n}_1}{d\theta} \approx 1 - \frac{\bar{n}_1}{F\tau_a} \approx 0, \qquad (27)$$

and consequently $\bar{n}_1 \approx F\tau_a$. The total number of monomers can be calculated from

$$\mathcal{N}_1 = \sum_y \bar{n}_1 y p(y) \mathcal{N} = \sum_y F y \tau_a p(y) \mathcal{N} = \langle F y \tau_a \rangle \mathcal{N} \quad (28)$$

with $p(y) = \sum_{s \geqslant i+1} p_s(y;\theta)$ and $\mathcal{N}$ the total number of islands. Defining the scaled gap size, $\ell = y/\bar{y} \approx yN$, from Eqs. (26) and (28) it is possible to show that [38]

$$NN_1 = \frac{1}{\Re}\left(\frac{\langle \ell^3 \rangle}{12N} + \frac{l_a \langle \ell^2 \rangle}{2}\right). \qquad (29)$$

The relation between the densities and the capture kernel $\bar{\sigma}$ in the A regime can be extracted from the rate equation (5), resulting in

$$\Re\bar{\sigma}NN_1 \approx 1. \qquad (30)$$

Then, from Eqs. (29) and (30) we found

$$\bar{\sigma} = \frac{12N}{\langle \ell^3 \rangle + 6\langle \ell^2 \rangle l_a N}. \qquad (31)$$

Equation (31) agrees with the results found in [38]. Note that for zero and small barriers $\bar{\sigma} \propto N$, while for large barriers

$\bar{\sigma} \propto l_a^{-1}$. Furthermore, τ_a and consequently $\bar{\sigma}$ are single-particle properties which do not depend on i. Thus, Eq. (31) can be used for arbitrary critical nucleus size [38].

As mentioned above, the evaluation of $\sigma_s(y)$ is a requirement to describe $P(s)$. To accomplish that, we focus on the time evolution of the local density of monomers $n_1(x,\theta)$ at the position x inside a single gap with length y. Explicitly, we have

$$\frac{\partial n_1(x,\theta)}{\partial \theta} = 1 + \Re\frac{\partial^2 n_1(x,\theta)}{\partial x^2} - \Re\frac{n_1(x,\theta)}{\xi_u^2}, \qquad (32)$$

with boundary conditions at gap edges

$$n_1(0,\theta) = l_a\frac{\partial n_1(0,\theta)}{\partial x},$$

$$n_1(y,\theta) = -l_a\frac{\partial n_1(y,\theta)}{\partial x}. \qquad (33)$$

The three terms in the right side of Eq. (32) represent deposition, diffusion of monomers, and nucleation, respectively. Note that for $l_a = 0$ and $l_a \to \infty$, Eqs. (33) represent absorbing and reflecting boundaries, respectively. In the former case, the monomers are captured by an island once they reach the interaction range. In contrast, for large barriers, the monomers need many attempts before being incorporated into an island. The average of the local monomer density in all the gaps, $\bar{n}_1$, is related with N_1 according to $N_1 = \gamma \bar{n}_1$. Then, multiplying Eq. (7) by γ and subtracting Eq. (32), we arrive at

$$\frac{\partial^2 n_1(x,\theta)}{\partial x^2} \approx \xi_u^{-2}\left(n_1(x,\theta) - \frac{\alpha^2}{\gamma}N_1\right), \qquad (34)$$

where $\alpha^2 = \xi_u^2/\xi^2$ and the approximation $dN_1/d\theta \approx \gamma\,\partial n_1/\partial\theta$ has been used to eliminate the coverage dependence. The solution of Eq. (32) with boundary conditions (33) can be written as

$$n_1(x) = \frac{\alpha^2 N_1}{\gamma}\left(1 - \frac{\cosh{(\tilde{x} - \tilde{y}/2)}}{\cosh{(\tilde{y}/2)} + \tilde{l}_a \sinh{(\tilde{y}/2)}}\right), \quad (35)$$

with $\tilde{x} = \xi_u^{-1}x$, $\tilde{y} = \xi_u^{-1}y$, and $\tilde{l}_a = \xi_u^{-1}l_a$. As before, $\tilde{\sigma}_s(y)$ represents the local capture kernel of an island with size s and gap length y. Thus, $\tilde{\sigma}_s(y)$ can be calculated by equating the expression for the rate of capture of monomers by an island of size s given in Eq. (5), $D\tilde{\sigma}_s(y)N_1$, to the microscopic rate of capture $2D[\partial n_1/\partial x]_{x=0}$. This leads to the following
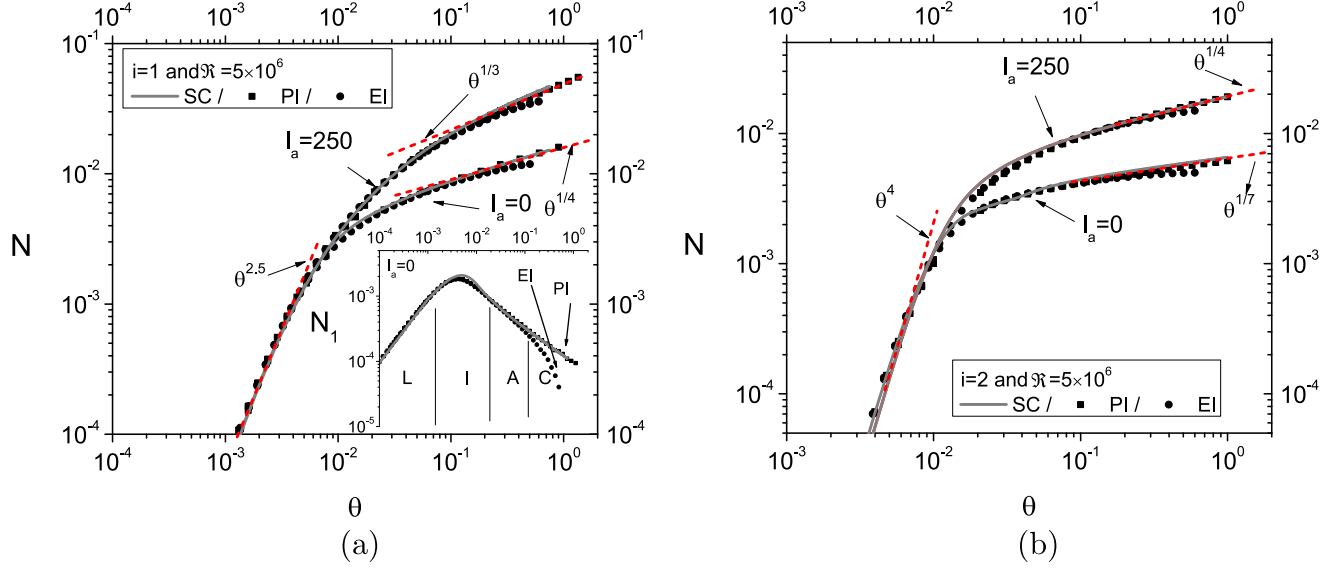
FIG. 3. Coverage evolution of the island density N for (a) $i = 1$ and (b) $i = 2$ with two different attachment barriers, $l_a = 0$ and $l_a = 250$, for both point (PI) and extended islands (EI). Dots correspond to kMC simulations, while continuous lines correspond to the SC approach. The ratio between diffusion constant and deposition rate was $\Re = 5 \times 10^6$. Dotted lines are included as a guide to the eye. The low coverage (L), intermediate (I), aggregation (A), and coalescence (C) regimes are indicated in the inset of panel (a), where the corresponding evolution of the (free) monomer density N_1 is shown.

expression:

$$\tilde{\sigma}_s(y) = \frac{2\alpha^2 \xi_u^{-1}}{\gamma} \frac{\tanh(\tilde{y}/2)}{1 + l_a \xi_u^{-1} \tanh(\tilde{y}/2)}. \tag{36}$$

Substituting Eq. (36) into (9) and replacing y by its average value $\bar{y} = \gamma/N$, we find another relation for the capture lengths

$$\xi^2 = \xi_u^2 \left(1 - \frac{2\xi_u N}{\gamma} \frac{\tanh\left(\frac{\gamma}{2\xi_u N}\right)}{1 + l_a \xi_u^{-1} \tanh\left(\frac{\gamma}{2\xi_u N}\right)} \right). \tag{37}$$

It is worth emphasizing that, as expected, Eqs. (36) and (37) reduce to those found for the DLA case $l_a = 0$ [14]. For large barriers, Eq. (37) reduces to $\xi_u \approx \xi$ implying $\alpha \approx 1$. Thus, in this regime $\tilde{\sigma}_s \approx 2/(\gamma l_a)$ and the dependence on the coverage and gap length vanishes as predicted by Eq. (31). For infinite barriers, $\bar{\sigma}_s = 0$ and the formation of islands with size larger than $i + 1$ becomes unlikely.

Furthermore, the kernel σ_u can be estimated as follows. From the RE equations, the density of islands increases according to $(i + 1)\Re \sigma_u N_1^{i+1}$, which can also be written in terms of the nucleation rate ω_n as $(i + 1)N \langle \bar{n}_1 y \omega_n(y) \rangle / F$. Thus, in the aggregation regime

$$\langle \bar{n}_1 y \omega_n(y) \rangle = D \sigma_u \frac{N_1^{i+1}}{N}. \tag{38}$$

On the other hand, the total nucleation rate inside a gap with length y, $\tilde{\omega}_n(y) = \bar{n}_1 y \omega_n(y)$, has been estimated in Ref. [37] for the A regime. For small and weak barriers, $\tilde{\omega}_n(y) \sim y^{2i+3}$ when $i > 1$ and $\tilde{\omega}_n(y) \sim y^4$ when $i = 1$. Thus, the average rates behave as

$$\langle \tilde{\omega}_n \rangle \sim \begin{cases} N_1^2 & \text{if } i = 1 \\ N_1^{(2i+3)/2} & \text{if } i > 1. \end{cases} \tag{39}$$

Finally, from Eqs. (29), (38), and (39), it is easy to show that for zero and weak barriers

$$\sigma_u \sim \begin{cases} N_1^{-1/2} & \text{for } i = 1 \\ \text{constant} & \text{for } i > 1. \end{cases} \tag{40}$$

Note that this result coincides with that found in Ref. [14] for $i = 1$ and $l_a = 0$. The case of large but finite barriers can be handled similarly by taking into account that $\tilde{\omega}_n(y) \sim y^{i+2}$ for all i [37]. Then, σ_u is a constant independent of the critical nucleus size. Following these results, for $i = 1$ and weak and zero barriers Eq. (40) implies

$$\sigma_u = \left(\frac{4}{\Re N_1} \right)^{1/2} \tag{41}$$

as shown in [14]. For $i = 1$ and strong barriers, σ_u follows Eq. (41) in the L regime and becomes constant in the A regime. For $i > 1$ and arbitrary barrier the nucleation kernel is coverage independent in the L and A regimes with a weak dependence in the I regime because the value of σ_u is not necessarily the same in both regimes. Consequently, for those sets of parameters we propose the empirical expression

$$\sigma_u = \frac{c_1 g(\theta) - c_2}{1 + \left(\frac{\theta}{c_3} \right)^{c_4}} + c_2, \tag{42}$$

where the c_i constants are fitting parameters and $g(\theta) = (4/\Re N_1)^{1/2}$ for $i = 1$ and $g(\theta) = 1$ for $i > 1$.

IV. RESULTS AND DISCUSSION

The coverage evolution of N for both point- and extended-island models in the DLA ($l_a = 0$) and ALA ($l_a = 250$) regimes are shown in Fig. 3, where kinetic Monte Carlo (kMC) simulations and the SC approach are contrasted. The low coverage (L), intermediate (I), aggregation (A), and coalescence (C)
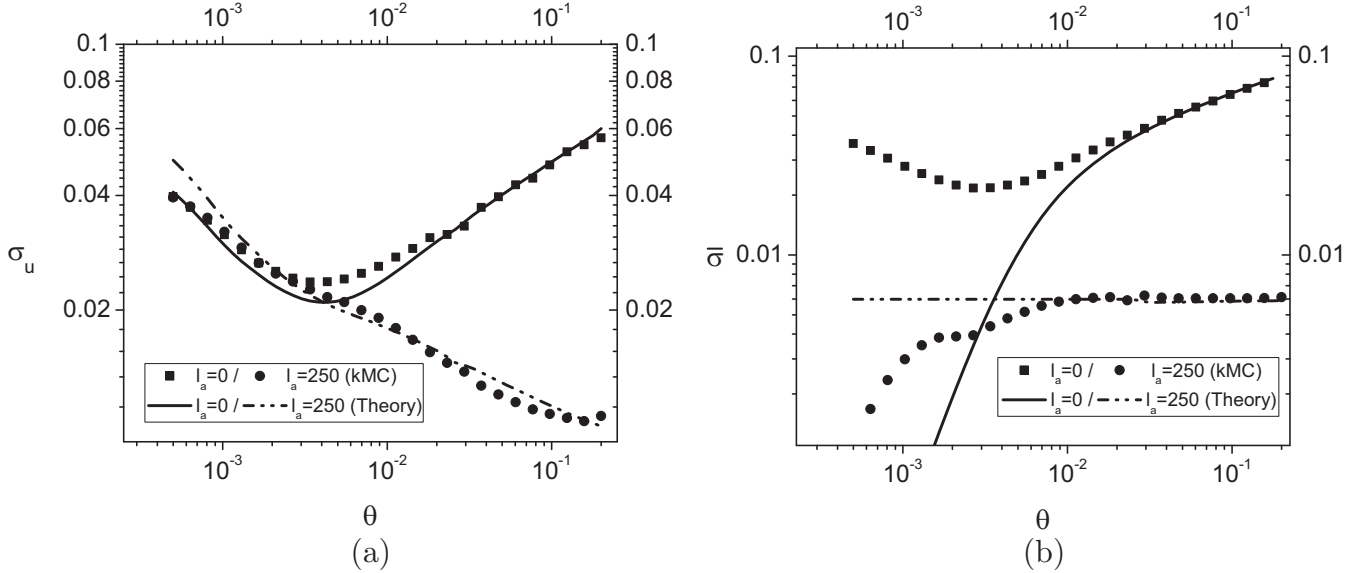
FIG. 4. Coverage evolution of the capture kernels (a) σ_u and (b) $\bar{\sigma}$ for point islands with $i = 1$ and two different attachment barriers: $l_a = 0$ and $l_a = 250$. In panel (a) lines correspond to Eq. (42), while in panel (b) to Eq. (31). In panel (a) the fit parameters used in Eq. (42) are $c_1 = 2$, $c_2 = c_4 = 0$ for $l_a = 0$, while $c_1 = 1.3$, $c_2 = 0.01$, $c_3 = 0.02$, and $c_4 = 1$ for $l_a = 250$.

regimes are indicated in the inset of Fig. 3(a). Note the power-law behavior $N \propto \theta^\beta$ in the L and A regimes. By definition the ϵ_a barrier does not affect nucleation; therefore in the L regime, which is dominated by nucleation, the evolution of N does not depend on l_a. However, in the A regime it does clearly depend on l_a; in fact, the growth exponent β defined by $N \propto \theta^\beta$ changes from $\beta = 1/4$ in the DLA regime to $\beta = 1/3$ in the ALA regime for $i = 1$ and from $\beta = 1/7$ to $\beta = 1/4$ in the case $i = 2$. As expected for large coverages, there are important differences between the point- and extended-island models inasmuch as in this regime the average island size is comparable to the average gap length, as shown in the inset of Fig. 3(a). As expected, the C regime arises for lower coverages in the extended-island model than in the point-island model where unphysical coverages $\theta > 1$ are possible.

Figure 4 shows the behavior of σ_u and $\bar{\sigma}$ as a function of the coverage for the point-island model with $i = 1$. Numerical results obtained from kMC simulations are compared to those from the analytical approximation. The kernel σ_u was calculated from Eq. (6), $\sigma_u = (dN/d\theta)/(\Re N_1^{i+1})$, using the kMC results to evaluate N_1 and $dN/d\theta$. The average kernel $\bar{\sigma}$ was calculated similarly using Eq. (5).

From Fig. 4(a) it is clear that in the L regime σ_u does not depend on l_a. However, there is an strong dependence in the A regime. For $l_a = 250$ the kernel σ_u seems to reach a constant value, while for $l_a = 0$ it increases with the coverage according to $\sigma_u \sim N_1^{-1/2}$ as predicted by Eq. (41). Due to the finite size of the islands, for the extended-island model an additional weak dependence on the coverage is found (not shown). For $i > 1$ and arbitrary values of l_a, $\bar{\omega}_n \propto N_1^{i+1}$ regardless of the value of l_a, implying that σ_u can be taken as a constant. Consequently, for $i > 1$ the local density of monomers inside a gap, $n_1(x)$, is in general well represented by the global average N_1.

According to Eq. (31), for arbitrary i, $\bar{\sigma} \sim N$ in the case of zero and weak barriers, while $\bar{\sigma} \sim 1/l_a$ for strong barriers. As shown in Fig. 4(b), these trends are also reproduced by the

kMC simulations. This result agrees with those obtained from Eqs. (36) and (37), which predicts $\xi_u \approx \xi \ll 1$ and $\tilde{\sigma}_s(y) \approx 2/(\gamma l_a)$ for large enough barriers. In this regime it is possible to neglect the island size dependence on the aggregation kernels. Moreover, given that the capture lengths are small in this regime, the density of monomers inside a gap can be considered homogeneous as predicted by Eq. (35).

For large barriers, the local density, $n_1(x, \theta)$, becomes almost homogeneous except close to the gap edges. This behavior is even more pronounced for large i. Consequently, the global density N_1 describes well $n_1(x, \theta)$ for all x far enough from the gap edges. Thus, we can expect that nucleation is almost uniform inside the gap and the nucleation capture kernel becomes almost independent on the local fluctuations of the monomer density. On the other hand, the aggregation kernel depends on the behavior of $\partial n_1(x, \theta)/\partial \theta$ close to the gap edges, as explained in the derivation of Eq. (36). Then, even in the case of strong barriers σ_s depends on the spatial fluctuations of the monomer density. Our results agree thoroughly with these observations.

In regard to the island size distribution, $P(s)$, Figs. 5–8 report the comparison between the obtained results from kMC simulations and those from the SC approach. Note that the horizontal axis indicates the island size once it has been normalized to its average value, i.e., $s \rightarrow s/\bar{s}$. The $P(s)$ data shown were evaluated in the A regime at coverage $\theta = 0.25$ for point islands (Figs. 5 and 6) and $\theta = 0.2$ for extended islands (Fig. 7). Two barriers were considered given by $l_a = 0$ and $l_a = 250$ for two different critical nucleus sizes, $i = 1$ and $i = 2$. In all cases the SC approach yields a good description of $P(s)$ regardless of the value of l_a. For point islands the results given by the MF approach, for which $\sigma_s \approx \bar{\sigma}$, are also included. For comparison purposes, the Amar and Family (AF) and the continuum RE (CRE) approaches given by Eqs. (15) and (16), respectively, are shown for the particular case of point islands with $i = 1$ (see Fig. 5). As shown, the island size
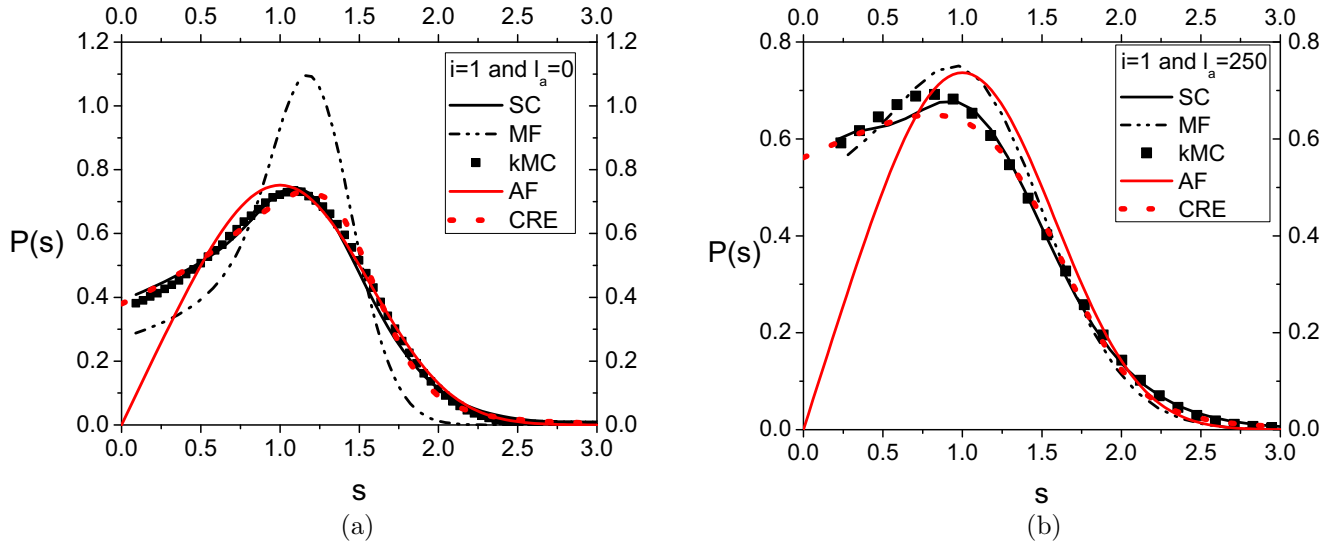
FIG. 5. Island size distribution for point islands with $i = 1$ and two different attachment barriers, (a) $l_a = 0$ and (b) $l_a = 250$. The parameters used are $\theta = 0.25$ and $\Re = 5 \times 10^6$. Symbols correspond to kMC simulations, while continuous and dotted lines correspond to the SC and MF approaches, respectively. For the AF result [Eq. (15)] the fit parameters are $A_i \approx 1.04$ and $B_i \approx 0.32$ for $l_a = 0$, while for $l_a = 250$ these are $A_i \approx 1.03$ and $B_i \approx 0.33$. For the CRE approach [Eq. (16)] we use $C_1 \approx 0.75$, $C_2 \approx 0.70$ and $C_1 \approx 0.7$, $C_2 \approx 0.68$ for $l_a = 0$ and $l_a = 250$, respectively. The fit parameters used in Eq. (42) are $c_1 = 2$ and $c_2 = c_4 = 0$ for $l_a = 0$ and $c_1 \approx 1.3$, $c_2 \approx 0.01$, $c_3 \approx 0.02$, and $c_4 \approx 1$ for $l_a = 250$.

distribution given by the MF approach deviates significantly from the kMC results even in the case $l_a = 250$. The same occurs in the case of extended islands (not shown). On the other hand, the AF approximation describes well the distribution for large values of s but deviates significantly from the kMC results for small values. For the considered set of parameters, the CRE approach gives good results for all island sizes. Unfortunately, the CRE requires the capture kernel σ_s as input which is not known explicitly. In Fig. 5 we used a third-order polynomial to approximate σ_s, whose coefficients were considered as fit parameters besides C_1 and C_2. Note that $l_a = 250$ represents a

large enough barrier to set the growth exponents of the densities N and N_1 in the limit values corresponding to the ALA regime [38]. However, even for this barrier the size of the islands plays a quite important role in the behavior of the capture kernels and has to be taken into account in order to describe $P(s)$ adequately.

For zero and weak barriers $P(s)$ is a monomodal distribution with a well-defined maximum, as can be seen in the (a) panels of Figs. 5–7. On the other hand, for large enough barriers the height of the maximum decreases in such a way that $P(s)$ becomes a monotonically decreasing distribution, as displayed
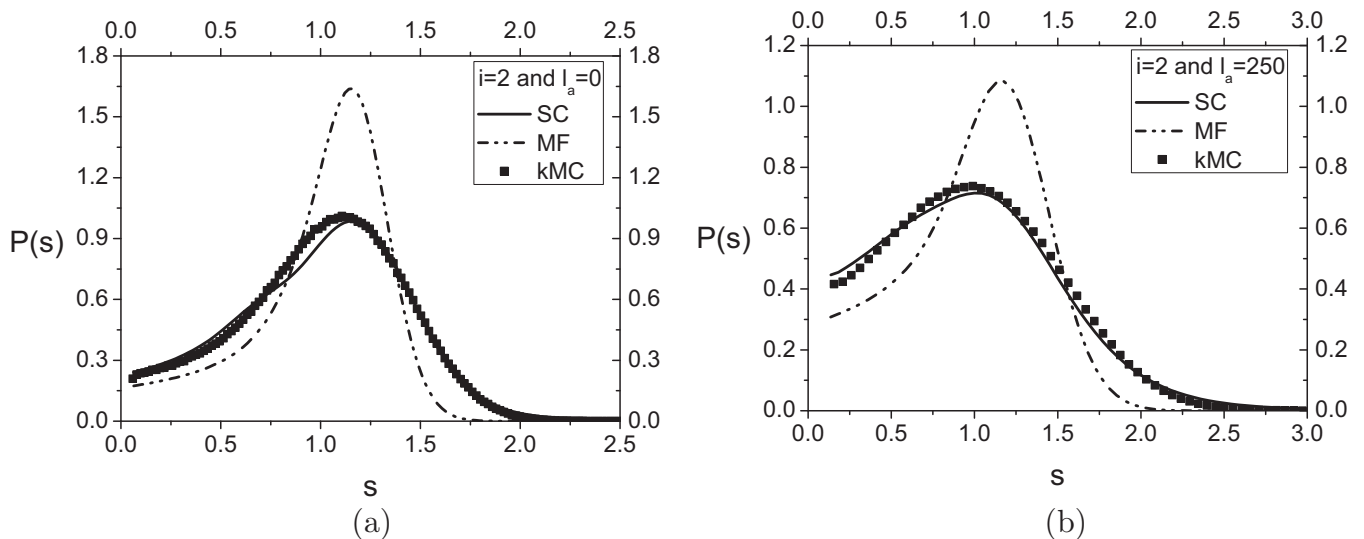
FIG. 6. Island size distribution for point islands with $i = 2$ and two different attachment barriers, (a) $l_a = 0$ and (b) $l_a = 250$. The parameters used are $\theta = 0.25$ and $\Re = 5 \times 10^6$. Symbols correspond to kMC simulations, while continuous and dotted lines correspond to the SC and MF approaches, respectively. The fit parameters used in Eq. (42) are $c_1 \approx 1$, $c_2 \approx 0.84$, $c_3 \approx 0.04$, and $c_4 \approx 13.36$ for $l_a = 0$, while $c_1 \approx 0.18$, $c_2 \approx 0.2$, $c_3 \approx 0.04$, and $c_4 \approx 10.39$ are for $l_a = 250$.
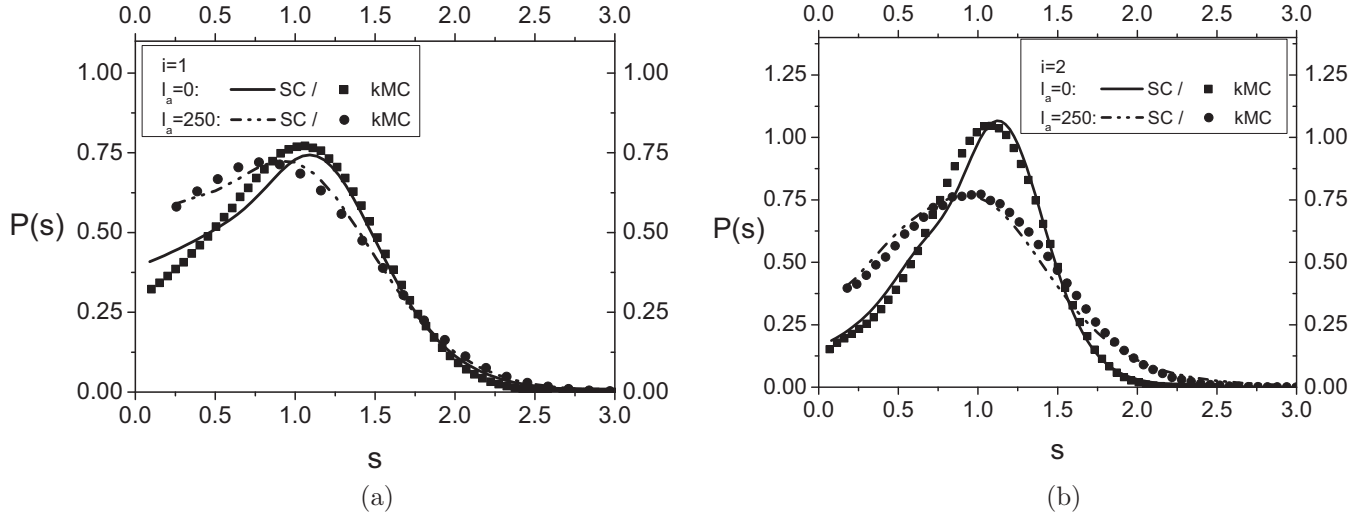
FIG. 7. Island size distribution for extended islands with (a) $i = 1$ and (b) $i = 2$, and two different attachment barriers, $l_a = 0$ and $l_a = 250$. The parameters used are $\theta = 0.2$ and $\Re = 5 \times 10^6$. Symbols correspond to kMC simulations, while lines correspond to the SC approach. In panel (a) the fit parameters used in Eq. (42) are $c_1 = 2$, $c_2 = c_4 = 0$ for $l_a = 0$, while $c_1 \approx 1$, $c_2 \approx 0.01$, $c_3 \approx 0.02$, and $c_4 \approx 3.1$ for $l_a = 250$. In panel (b) we used $c_1 \approx 0.25$, $c_2 \approx 1$, $c_3 \approx 0.025$, and $c_4 \approx 2.21$ for $l_a = 0$, while $c_1 \approx 0.23$, $c_2 \approx 0.31$, $c_3 \approx 0.07$, and $c_4 \approx 2.68$ for $l_a = 250$.

in Fig. 8(a). This is not an unexpected result inasmuch as the formation of large islands requires the aggregation of several monomers to small islands. The typical time of aggregation inside a gap of length y for large l_a values increases by a factor $6l_a/y$ with respect to the case without barriers. Thus, the formation of large islands requires a significantly much longer time in the case of large barriers than in the case of zero and weak barriers. Additionally, for large barriers $\tau_a \gg \tau_n$, so that nucleation events occur more often than aggregation ones. For a given coverage, this implies that the average island size decreases for large barriers in comparison to the case of weak and zero barriers. In fact, if $l_a \to \infty$, then the limit case

$P(s) \to \delta_{s,i+1}$ is obtained and only formation of islands with size $i + 1$ is found.

For a large but finite barrier, islands with size larger than $i + 1$ start to appear at coverages $\theta \approx F\langle \tau_a \rangle$. This defines the I regime where N_1 remains almost constant and $N \approx \theta/c$, where $c \geqslant i + 1$ and $c \to i + 1$ when $l_a \to \infty$, as shown in the insets of Fig. 8. For finite systems the time required to form islands larger than $i + 1$ may satisfy $\theta > 1$, which is not physically possible. For practical purposes, in those cases the barrier can be considered as infinite since the formation of islands with size larger than $i + 1$ is very unlikely. Naturally, in this regime the density of monomers can be considered homogeneous;
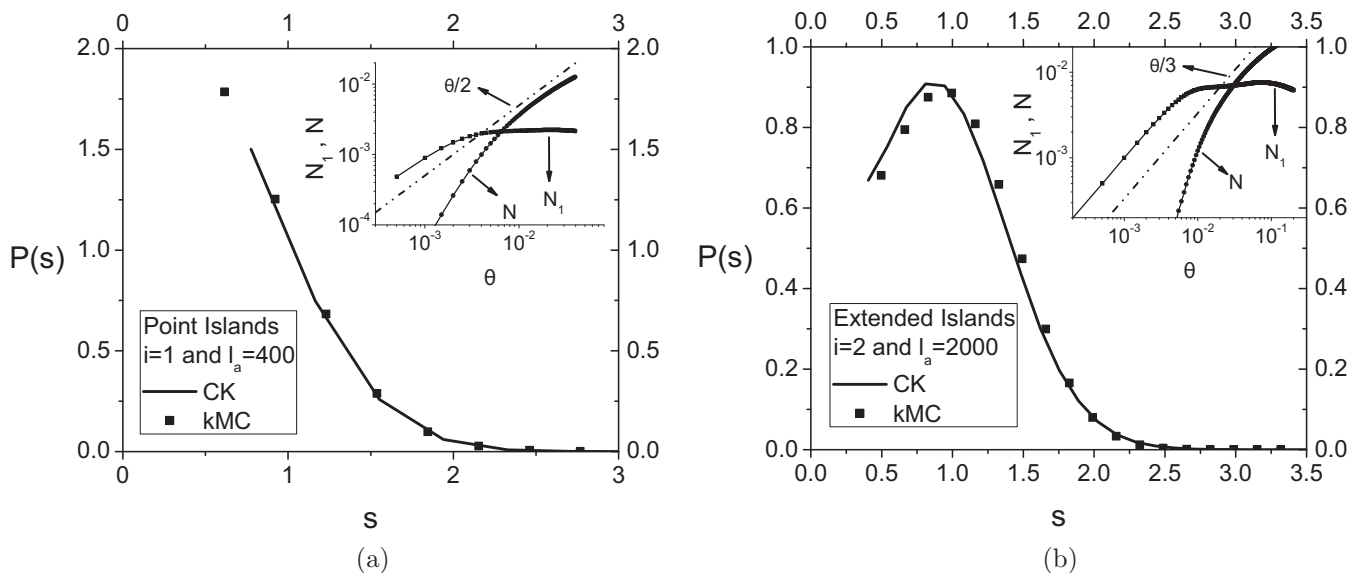
FIG. 8. Island size distribution for (a) point islands with $i = 1$ and $l_a = 400$, and for (b) extended islands with $i = 2$ and $l_a = 2000$. The solution of Eqs. (12) and (13) with constant kernels (CK) given by Eq. (14) is represented by the continuous line. Data were evaluated at $\theta = 0.02$ with $\Re = 5 \times 10^6$. Insets display the corresponding densities of monomers and islands in the intermediate regime.

consequently, σ_u and σ_s can be taken as constants and Eq. (14) can be used to describe $P(s)$. Figure 8 shows two examples, $i = 1$ with $l_a = 400$ and $i = 2$ with $l_a = 2000$. In both cases $\theta_c \approx 0.02$. The agreement between the kMC and Eq. (14) results is excellent.

As a final remark we want to point out that our model is simple, easy to implement, and can be used as a starting point to improve the analysis of experimental data where the standard models based on the DLA regime do not achieve satisfactory results. Naturally, 2D systems have quantitatively different behavior from the 1D model discussed here. Nevertheless, the SC approach used in the present work can be extended and applied to the experimentally relevant case of a 2D substrate.

APPENDIX: SOLUTION OF THE RE FOR CONSTANT KERNELS

Using the Laplace's transformation,

$$\tilde{N}_s(r) = \mathcal{L}[N_s(\tau)](r) = \int_0^\infty d\tau \, \exp(-\tau \, r) N_s(\tau),$$

Eqs. (12) and (13) take the form

$$(r + 1)\tilde{N}_{i+1} = \frac{\sigma_u}{\sigma} \mathcal{L}[N_1^i](r) \tag{A1}$$

and

$$(r + 1)\tilde{N}_s = \tilde{N}_{s-1} \quad \text{for } s > i + 1, \tag{A2}$$

where it has been assumed $\tilde{N}_s(0) = 0$ for $s \geqslant i + 1$. Equations (A1) and (A2) form a closed set of equations which can be solved recursively. The explicit solution of $\tilde{N}_s$ is

$$\tilde{N}_{s+i+1} = \frac{1}{(r + 1)^s} \frac{\sigma_u}{\sigma} \mathcal{L}[N_1^i](r). \tag{A3}$$

Noticing that the last equation can be interpreted as the Laplace's transform of a convolution product, it is possible to write

$$N_{s+i+1} = \frac{\sigma_u}{\sigma} \int_0^\tau dr \, \exp(-r) \left(\frac{r^s}{s!}\right) N_1^i(\tau - r)$$

$$= \frac{\sigma_u}{s! \, \sigma} \int_0^\tau dr \, \exp(-r + s \, \ln r) N_1^i(\tau - r). \tag{A4}$$

In order to make analytical progress we focus in the limit of $\tau \approx s$ with $\tau, s \to \infty$ and $z = (s - \tau)/\sqrt{2\tau}$ finite. In this case, it is possible to approximate $\exp(-r + s \, \ln r)$ around the maximum $r = s$ by a Gaussian function. This leads to

$$N_{s+i+1} \approx \frac{\sigma_u}{\sigma \sqrt{2\pi s}} \int_0^\tau dr \, \exp\left[-\frac{(r - s)^2}{2s}\right] N_1^i(\tau - r), \tag{A5}$$

where the approximation $s! \approx \sqrt{2\pi s} \, s^s/e^s$ has been used. Making the change of variable $r = s - v\sqrt{2\tau}$ in Eq. (A5) we obtain

$$N_{s+i+1} \approx \frac{\sigma_u}{\sqrt{\pi}\sigma} \int_z^\infty dv \, \exp(-v^2) N_1^i[\sqrt{2\tau}(v - z)]. \tag{A6}$$

Finally, in the aggregation regime the average monomer density behaves as $N_i \propto \tau^{-i\chi/(1+\chi)}$ with χ the growth exponent of N_1 [38]. Using this expression on Eq. (A6) we found Eq. (14).

[1] H. J. Fecht, Europhys. News. **28**, 89 (1997).

[2] F. Shi, Y. Shim, and J. G. Amar, Phys. Rev. E **79**, 011602 (2009).

[3] J. G. Amar and M. N. Popescu, Phys. Rev. B **69**, 033401 (2004).

[4] M. N. Popescu, J. G. Amar, and F. Family, Phys. Rev. B **58**, 1613 (1998).

[5] F. Shi, Y. Shim, and J. G. Amar, Phys. Rev. B **71**, 245411 (2005); Phys. Rev. E **74**, 021606 (2006).

[6] C. Ratsch, A. Zangwill, P. Šmilauer, and D. D. Vvedensky, Phys. Rev. Lett. **72**, 3194 (1994).

[7] P. A. Mulheran and J. A. Blackman, Phys. Rev. B **53**, 10261 (1996).

[8] J. W. Evans and M. C. Bartelt, Phys. Rev. B **63**, 235408 (2001).

[9] C. Ratsch, Y. Landa, and R. Vardavas, Surf. Sci. **578**, 196 (2005).

[10] V. I. Tokar and H. Dreyssé, Phys. Rev. B **80**, 161403(R) (2009).

[11] J. W. Evans and M. C. Bartelt, Phys. Rev. B **66**, 235410 (2002).

[12] J. A. Blackman and P. A. Mulheran, Phys. Rev. B **54**, 11681 (1996).

[13] M. N. Popescu, J. G. Amar, and F. Family, Phys. Rev. B **64**, 205404 (2001).

[14] J. G. Amar, M. N. Popescu, and F. Family, Surf. Sci. **491**, 239 (2001).

[15] C. Thelander, P. Agarwal, S. Brongersma, J. Eymery, L. F. Feiner, A. Forchel, M. Scheffler, W. Riess, B. J. Ohlsson, U. Gosele, and L. Samuelson, Mater. Today **9**, 28 (2006).

[16] W. Wang, F. Lv, B. Lei, S. Wan, M. Luo, and S. Guo, Adv. Mater. **28**, 10117 (2016).

[17] F. Patolsky, G. Zheng, and C. M. Lieber, Nanomedicine **1**, 51 (2006).

[18] K. Morgenstern, J. Kibsgaard, J. V. Lauritsen, E. Laegsgaard, and F. Besenbacher, Surf. Sci. **601**, 1967 (2007).

[19] V. Repain, S. Rohart, Y. Girard, A. Tejeda, and S. Rousset, J. Phys.: Condens. Matter **18**, S17 (2006).

[20] J. R. Albia and M. A. Albao, Phys. Rev. E **95**, 042802 (2017).

[21] M. A. Albao, M. M. R. Evans, J. Nogami, D. Zorn, M. S. Gordon, and J. W. Evans, Phys. Rev. B **72**, 035426 (2005).

[22] J. Javorský, M. Setvín, I. Ošt'ádal, P. Sobotík, and M. Kotrla, Phys. Rev. B **79**, 165424 (2009).

[23] M. Kučera, P. Kocán, P. Sobotík, K. Majer, and I. Ošt'ádal, Phys. Rev. B **96**, 045430 (2017).

[24] T.-C. Chang, I.-S. Hwang, and T. T. Tsong, Phys. Rev. Lett. **83**, 1191 (1999).

[25] T.-C. Chang, K. Chatterjee, S.-H. Chang, Y.-H. Lee, and I.-S. Hwang, Surf. Sci. **605**, 1249 (2011).

[26] I.-S. Hwang, T. C. Chang, and T. T. Tsong, Phys. Rev. Lett. **80**, 4229 (1998).

[27] I.-S. Hwang, T. C. Chang, and T. T. Tsong, Jpn. J. Appl. Phys. **39**, 4100 (2000).

[28] S. M. Binz, M. Hupalo, X. Liu, C. Z. Wang, W.-C. Lu, P. A. Thiel, K. M. Ho, E. H. Conrad, and M. C. Tringides, Phys. Rev. Lett. **109**, 026103 (2012).

[29] H. Jónsson, Annu. Rev. Phys. Chem. **51**, 623 (2000).

[30] C. Ratsch and J. A. Venables, J. Vac. Sci. Technol. A **21**, S96 (2003).

[31] E. Loginova, N. C. Bartelt, P. J. Feibelman, and K. F. McCarty, New J. Phys. **10**, 093026 (2008).

[32] E. Loginova, N. C. Bartelt, P. J. Feibelman, and K. F. McCarty, New J. Phys. **11**, 063046 (2009).

[33] H. S. Mok, A. Ebnonnasir, Y. Murata, S. Nie, K. F. McCarty, C. V. Ciobanu, and S. Kodambaka, Appl. Phys. Lett. **104**, 101606 (2014).

[34] J. Ning, D. Wang, D. Han, Y. Shi, W. Cai, J. Zhang, and Y. Hao, J. Cryst. Growth **424**, 55 (2015).

[35] J. Park, J. Lee, J.-H. Choi, D. K. Hwang, and Y.-W. Song, Sci. Rep. **5**, 11839 (2015).

[36] D. L. González, Revista de Cienc. **18**, 81 (2014).

[37] D. L. González, J. Phys. A: Math. Theor. **50**, 035001 (2017).

[38] D. L. González, A. Pimpinelli, and T. L. Einstein, Phys. Rev. E **96**, 012804 (2017).

[39] C. Castellano and P. Politi, Phys. Rev. Lett. **87**, 056102 (2001).

[40] P. Politi and C. Castellano, Phys. Rev. E **66**, 031605 (2002).

[41] P. Politi and C. Castellano, Phys. Rev. E **66**, 031606 (2002).

[42] D. L. González, A. Pimpinelli, and T. L. Einstein, Phys. Rev. E **84**, 011601 (2011).

[43] K. P. O'Neill, M. Grinfeld, W. Lamb, and P. A. Mulheran, Phys. Rev. E **85**, 021601 (2012).

[44] P. A. Mulheran, K. P. O'Neill, M. Grinfeld, and W. Lamb, Phys. Rev. E **86**, 051606 (2012).

[45] M. Grinfeld, W. Lamb, K. P. O'Neill, and P. A. Mulheran, J. Phys. A: Math. Theor. **45**, 015002 (2012).

[46] M. Körner, Mario Einax, and P. Maass, Phys. Rev. B **86**, 085403 (2012).

[47] J.-S. Lee, S. Sugou, and Y. Masumoto, J. Cryst. Growth **205**, 467 (1999).

[48] J.-S. Lee, M. Sugisaki, H.-W. Ren, S. Sugou, and Y. Masumoto, Physica E **7**, 303 (2000).

[49] P. Gambardella, H. Brune, K. Kern, and V. I. Marchenko, Phys. Rev. B **73**, 245425 (2006).

[50] V. I. Tokar and H. Dreyssé, Phys. Rev. B **76**, 073402 (2007).

[51] F. Picaud, C. Ramseyer, C. Girardet, H. Brune, and K. Kern, Surf. Sci. **553**, L68 (2004).

[52] Y. Han, É. Gaudry, T. J. Oliveira, and J. W. Evans, J. Chem. Phys. **145**, 211904 (2016).

[53] R. C. Ball, D. A. Weitz, T. A. Witten, and F. Leyvraz, Phys. Rev. Lett. **58**, 274 (1987).

[54] H. Kallabis, P. L. Krapivsky, and D. E. Wolf, Eur. Phys. J. B **5**, 801 (1998).

[55] J. Krug, P. Politi, and T. Michely, Phys. Rev. B **61**, 14037 (2000).

[56] P. Meakin and F. Family, Phys. Rev. A **38**, 2110 (1988).

[57] Z. Zhang and M. G. Lagally, Science **276**, 377 (1997).

[58] T. Potocar, S. Lorbek, D. Nabok, Q. Shen, L. Tumbek, G. Hlawacek, P. Puschnig, C. Ambrosch-Draxl, C. Teichert, and A. Winkler, Phys. Rev. B **83**, 075423 (2011).

[59] L. Tumbek, C. Gleichweit, K. Zojer, and A. Winkler, Phys. Rev. B **86**, 085402 (2012).

[60] D. Kandel, Phys. Rev. Lett. **78**, 499 (1997).

[61] V. I. Tokar and H. Dreyssé, Phys. Rev. E **92**, 062407 (2015).

[62] D. Walton, J. Chem. Phys. **37**, 2182 (1962).

[63] H. Ibach, *Physics of Surfaces and Interfaces* (Springer, Berlin, 2006).

[64] J. G. Amar and F. Family, Phys. Rev. Lett. **74**, 2066 (1995).

[65] M. C. Bartelt and J. W. Evans, Phys. Rev. B **46**, 12675 (1992).

[66] J. G. Amar, F. Family, and P.-M. Lam, Phys. Rev. B **50**, 8781 (1994).

[67] M. C. Bartelt and J. W. Evans, Phys. Rev. B **54**, R17359 (1996).